Hindawi
Wireless Communications and Mobile Computing
Volume 2022, Article ID 3631134, 9 pages
https://doi.org/10.1155/2022/3631134

Research Article

Research on Mono-Pulse Beam Angle Tracking Algorithm of Phased Array Antenna Based on CKF

Liu Xuan, Li Ruo-xin, and He Yi-feng

China Academy of Space Technology, Xi'an 710100, China

Correspondence should be addressed to Liu Xuan; liuxuan0229@qq.com

Received 24 May 2022; Accepted 21 July 2022; Published 22 August 2022

Academic Editor: Haitao Xu

Phased array antenna beam tracking and communication system based on mono-pulse system is an alternative satellite-to-earth communication technology solution for future planetary spacecraft, which meets the mission requirements of agile scanning, multimode, wide field of view, and small size. This paper firstly outlines the technical scheme of mono-pulse angle tracking based on the planar phased array antenna. A simplified mathematical model of angle measurement is summarized. Secondly, the beam pointing of the spacecraft communication antenna is frequently affected by the attitude and presents a nonlinear dynamic change. A robust two-dimensional angular tracking filtering algorithm based on cubature Kalman filter (CKF) is proposed, in order to solve this complex high-order nonlinear dynamic estimation problem. Finally, the comprehensive performance of the proposed algorithm is simulated and analyzed under two conditions of stable flight and high dynamic flight of the spacecraft. When the angular velocity is within 4°/s, the tracking accuracy can be better than 0.65°, and the tracking accuracy will be better than 1° when the angular velocity is within 8°/s. Compared with the basic CKF algorithm, the robust CKF tracking accuracy is significantly improved, while the resource consumption is slightly reduced. The research results can provide reference for the engineering implementation of related fields in the future.

1. Introduction

The satellite-ground communication link is a necessary condition to ensure the success of the spacecraft's on-orbit mission. With the in-depth and extensive development of China's deep space exploration activities, more requirements have been placed on the satellite-to-earth communication system. Taking the future lunar manned exploration mission as an example, the mission requires a stable and reliable satellite-to-ground two-way communication link under the conditions of a huge field of view and long distance. The communication scenarios of the entire mission involve various situations such as low-Earth orbit, transfer orbit, lunar landing, and lunar surface movement. Due to the attitude maneuver of the spacecraft during the mission, the antenna pointing is deflected, which in turn causes fluctuations in the received power, resulting in a decrease in the quality of information transmission and even communication interruption. Therefore, the satellite-to-ground communication system needs to have the function of adaptive adjustment of the antenna beam direction. Under the resource constraints of the spacecraft platform, the phased array tracking communication system based on the mono-pulse system has significant technical advantages. For the direction finding of phased array antennas, the mono-pulse technique based on sum-difference beams is widely used and has the best comprehensive performance.

Angle tracking filtering is the key function in sum-differential beam angle measurement systems of phased array antenna, which determines the dynamic performance and accuracy of the entire system. The core problem is to design an efficient and accurate angle tracking algorithm. Future deep space exploration missions put forward requirements for the angle tracking function of the satellite-ground communication link system: (1) Strong robustness, spacecraft EMC environment, space irradiation, space force, and heat environment will lead to the prior model of orbit and attitude inaccurate; (2) although attitude maneuver of greater magnitude and speed occur at high frequencies, uninterrupted communication links are required; and (3) the computing resources of the spacecraft platform are

limited. Thus, it is necessary to focus on the complexity of the algorithm and the requirements of real-time angle forecast. In addition, the angle tracking filtering algorithm should be able to match the operation of the single-pulse angle measurement closed-loop system.

Based on the above engineering background, the research content of this paper focuses on the single-pulse angle measurement model and the angle tracking filtering algorithm. The basic framework of the CKF algorithm is combined with the two-dimensional angle measurement mathematical model. Through the improvement of robustness, a suitable spacecraft is proposed. Angle tracking filtering algorithm of mono-pulse angle measurement system under attitude maneuver condition and the feasibility and effectiveness of the algorithm are studied.

2. Mono-Pulse Angle Tracking System

2.1. System Structure. In the mono-pulse angle tracking system based on phased array antenna, the angle deviation error signal output by the tracking receiver is sent to the wave control device, and the wave control code produced by the wave control device drives the antenna beam to point in the direction of decreasing angle error, so that the antenna beam points precisely at the target continuously. Single-pulse technology is divided into two basic types: "amplitude comparison" and "phase comparison." The phase comparison method has the advantages of high precision and simple engineering design and is the preferred solution.

The coordinate diagram of the mono-pulse ratio phase angle measurement based on the planar phased array antenna is shown in Figure 1. The entire plane is equally divided into four subarrays ABCD to generate sum-difference beams. Suppose the antenna aperture is located on the XOY plane, OZ is the antenna electrical axis, and the input signal point is located on the spherical surface with the origin of O, the angle between the target axis OE and the OZ axis is, and the angle range is -90°~90°. The projection of the incident point on the XOY plane of the antenna aperture is point G, the angle between the vector OG and the OX axis is recorded as φ, and the angle range is -90°~90°.

The schematic diagram of the entire automatic tracking system is shown in Figure 2, which is divided into three core parts:

(1) Phased array antenna. The beam forming is completed according to the wave control code. The sum beam, the azimuth difference beam, and the elevation difference beam are, respectively, formed based on the amplitude weighting network in the receiving antenna

(2) Capture the loop. Perform fast Fourier transform on the sum signal from the receiving antenna, and detect the energy and frequency. Then, according to the detection results, the polling traversal of the antenna scanning angle is driven to achieve full coverage of the specified airspace

(3) Tracking loop. Complete the vector synthesis of the azimuth difference and elevation difference signals. The detected frequency deviation of the received signal is used to assist the four-phase modulator and the angle error extraction module. According to the angular error level and the parameters of the phased array antenna element distribution, the azimuth and elevation deviations are calculated. Then, tracking filtering, pointing angle synthesis, coordinate conversion, wave control code generation, and then driving the transmit/receive antenna to point to the target are completed in sequence

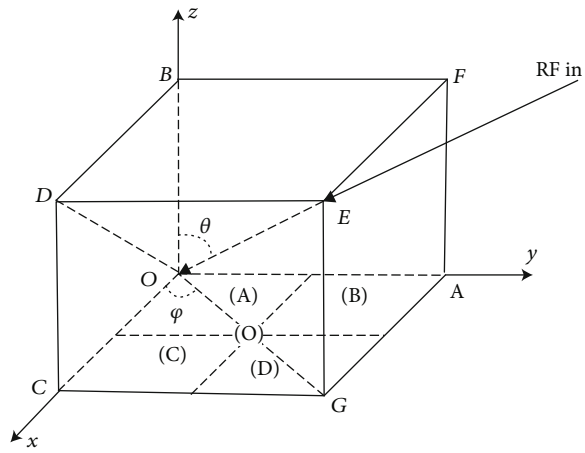

Figure 1: Angle measurement coordinate diagram of planar-phased array antenna.

2.2. Simplified Goniometric Algorithm. The direction vector of the incoming signal based on the coordinate system of Figure 1, [1] is

$$r = (\sin\varphi\cos\theta, \sin\theta, \cos\varphi\cos\theta). \tag{1}$$

Taking point (O) as a reference, the position coordinates of the other four subarray quadrants are

$$\begin{aligned} P_A &= \left[D_x, D_y, 0\right], \\ P_B &= [D_x, -D_x, 0], \\ P_C &= \left[\text{-}D_x, D_y, 0\right], \\ P_D &= \left[\text{-}D_x, \text{-}D_y, 0\right]. \end{aligned} \tag{2}$$

Assume that the planar phased array antenna is a uniform array, so $D_x = D_y = D$. If the current beam pointing angle is (θ_0, φ_0) and the magnitude direction of the array is $F(\theta, \varphi)$, then, the amplitude patterns of the sum and difference beams are given based on the sum-difference operation of the received signals of the four subarrays as:

$$\begin{aligned} F_\Sigma &= F(\theta, \varphi) \cdot 4\cos a\cos b, \\ F_{\Delta A} &= F(\theta, \varphi) \cdot 4j\cos a\sin b, \\ F_{\Delta E} &= F(\theta, \varphi) \cdot j\sin a\cos b. \end{aligned} \tag{3}$$

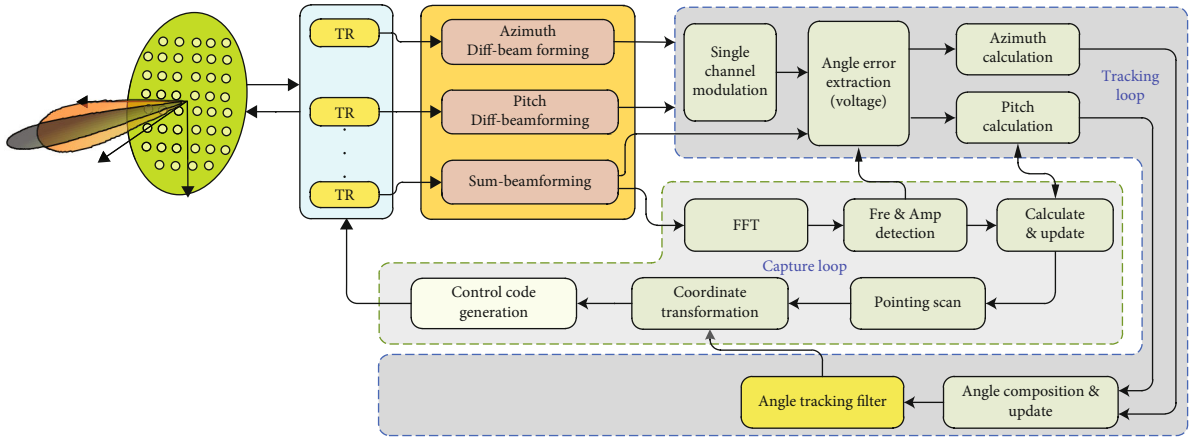

Figure 2: The block diagram of angle capture and tracking of the mono-pulse technology.

Among them, $a = 2\pi D(\sin\theta - \sin\theta_0)/\lambda$, $b = 2\pi D(\sin\varphi \cos\theta - \sin\varphi_0 \cos\theta_0)/\lambda$, and the amplitude ratio of sum-difference beam is:

$$\frac{\text{imag}(F_{\Delta A})}{F_\Sigma} = \tan\left(\frac{2\pi D}{\lambda}(\sin\varphi\cos\theta - \sin\varphi_0\cos\theta_0)\right),$$
$$\frac{\text{imag}(F_{\Delta E})}{F_\Sigma} = \tan\left(\frac{2\pi D}{\lambda}(\sin\theta - \sin\theta_0)\right). \tag{4}$$

If the difference between the current beam incident angle and the actual beam pointing angle is $(\Delta\theta, \Delta\varphi)$, with proper parameter design to match the pattern of the phased array antenna, the angular pull range can be reduced to $\pm\alpha/2$ (α is 3 dB beamwidth, about 3° in the background project). At this time, the angle difference is relatively small, so it can be simplified:

$$\sin(\theta) = \sin(\theta_0 + \Delta\theta) \approx \sin\theta_0 + \Delta\theta\cos\theta_0 \approx \Delta\theta\cos\theta_0, \tag{5}$$

$$\begin{aligned}\sin\varphi\cos\theta &= \sin(\varphi + \Delta\varphi)\cos(\theta + \Delta\theta) \approx \sin\varphi_0\cos\theta_0 \\ &\quad - \Delta\theta\sin\varphi_0\sin\theta_0 + \Delta\varphi\cos\varphi_0\cos\theta_0 \\ &\Rightarrow \sin\varphi\cos\theta - \sin\varphi_0\cos\theta_0 \\ &= \Delta\varphi\cos\varphi_0\cos\theta_0 - \Delta\theta\sin\varphi_0\sin\theta_0.\end{aligned} \tag{6}$$

In the above simplified processing, $\Delta\varphi\Delta\theta\cos\varphi_0\sin\theta_0$ is discarded, and $\sin\Delta\theta \approx \Delta\theta, \cos\Delta\theta \approx 1$. So the sum-difference beam amplitude ratio can be simplified as follows:

$$\frac{\text{imag}(F_{\Delta A})}{F_\Sigma} = \tan\left(\frac{2\pi D}{\lambda}(\Delta\varphi\cos\varphi_0\cos\theta_0 - \Delta\theta\sin\varphi_0\sin\theta_0)\right),$$
$$\frac{\text{imag}(F_{\Delta E})}{F_\Sigma} = \tan\left(\frac{2\pi D}{\lambda}(\Delta\theta\cos\theta_0)\right). \tag{7}$$

The declination angle is easy to solved as:

$$\Delta\theta = \frac{\lambda}{2\pi D\cos\theta_0}\arctan\left(\frac{\text{imag}(F_{\Delta A})}{F_\Sigma}\right), \tag{8}$$

$$\Delta\varphi = \frac{\lambda}{2\pi D\cos\theta_0\cos\varphi_0}\arctan\left(\frac{\text{imag}(F_{\Delta\Sigma})}{F_\Sigma}\right) + \Delta\theta\tan\theta_0\tan\varphi_0. \tag{9}$$

So, according to the level ratio of the pitch difference and the sum, and that of azimuth difference and the sum, combined with the phased array antenna front size D and the current beam pointing angle, the pitch angle difference and the azimuth angle difference can be obtained easily.

The rms angle error of a mono-pulse measurement in a thermal noise environment is evaluated in terms of the mono-pulse difference slope, as shown in Figures 3 and 4 in which the carrier-to-noise ratio of the incident signal is 65 dBHz. k_m is determined from the measured Σ and Δ patterns as the derivative of the ratio of the difference pattern divided by sum pattern to the beamwidth divided by sum beamwidth:

$$k_m = \frac{d(\Delta/\Sigma)}{d(\theta_\Delta/\theta_\Sigma)}. \tag{10}$$

3. Robust CKF Algorithm

According to formulas (8) and (9), combined with the tracking loop process in Figure 1, it is necessary to accurately estimate the timing change of the synthetic angle in order to achieve close tracking of the incoming wave and ensure accurate beam pointing, in which angle tracking algorithm plays a key role. The problem of tracking target orientation is a typical nonlinear filtering problem, which needs to estimate the time-varying and unobservable states of nonlinear dynamic systems from noisy observations. For the nonlinear problem of the coupling of attitude and beam direction of the spacecraft under complex orbital conditions, there are usually poor observability, large initial error in state estimation, high real-time requirements, and frequent interference from the space environment. State estimation algorithms are required. It has

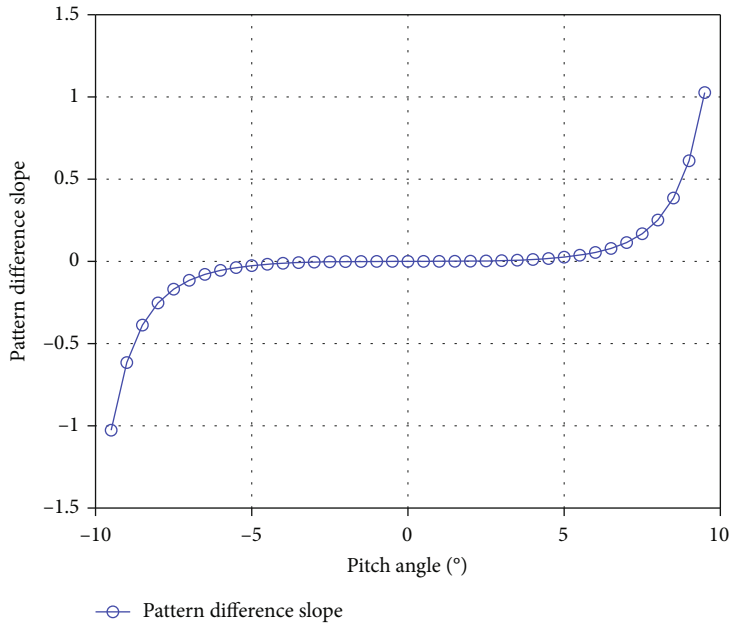

Figure 3: Simulation results of sum-difference beam pattern.

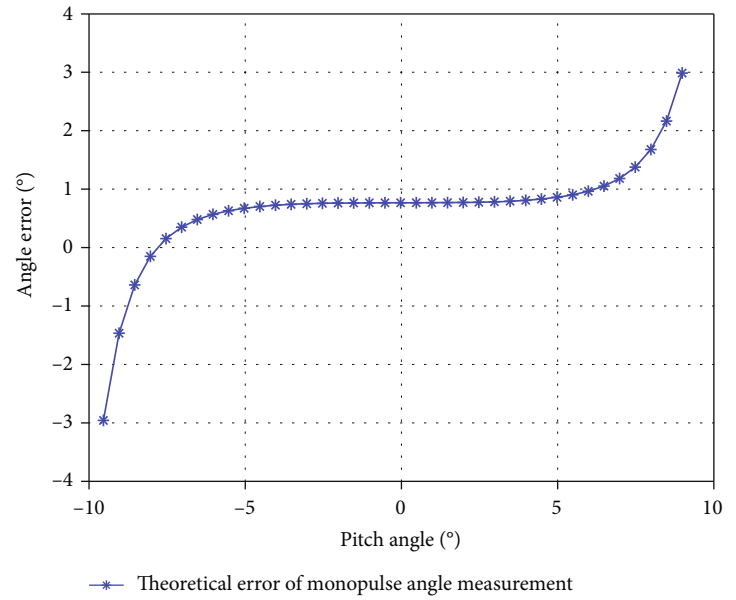

Figure 4: Mono-pulse angle tracking error curve based on beam pattern.

the advantages of fast convergence, strong robustness, and high estimation accuracy. EKF, UKF, PF, and CKF are often used to deal with this problem. Literature [2] theoretically proves that for nonlinear high dynamic Gaussian tracking problem, CKF is superior to UKF and EKF in terms of accuracy and robustness. Literature [3, 4] obtained from the actual simulation that CKF has an algorithm time. The consumption is lower than the conclusion of UKF, PF, and UPF. Accordingly, based on the CKF framework, a robust two-dimensional angle tracking filtering algorithm based on the volumetric Kalman filter (CKF) is proposed in the paper, integrating the two-dimensional angle observation equation and the robustness enhancement method.

The volumetric Kalman filter algorithm CKF was first proposed by Arasaratnam I and Haykin S in 2009, which belongs to the sampling filtering solution under the Bayesian estimation framework [4, 5]. Based on the third-order spherical radial volume criterion, CKF uses a set of volume points to approximate the state mean and covariance of a nonlinear system with additional Gaussian noise. It is the closest approximation algorithm to Bayesian filtering in theory. Its core is to solve the integral solution of "non-linear function × Gaussian probability density function."

In the iterative operation of the basic CKF algorithm, the state estimation covariance matrix $P_{k|k}$ and the one-step

Inputs: Observations, probability functions, noise, number of simulation points: $\hat{x}_k, P_k, Q, R, N$
Output: Estimated observations: $\hat{x}_{k+1}$
for k =1,2,…,N

// State prediction: calculate the predicted value of the state and the error covariance //

1) Cholesky decomposition of error covariance: $P_{(k-1)|(k-1)} = S_{(k-1)|(k-1)} S^T_{(k-1)|(k-1)}$

2) Calculate volume points: $x_{i,(k-1)|(k-1)} = S_{(k-1)|(k-1)}\xi_i + \hat{x}_{i,(k-1)|(k-1)}$

3) Spread volume points: $x^*_{i,k|(k-1)} = f\left(x_{i,(k-1)|(k-1)}\right)$

4) State prediction at time k: $\hat{x}_{k|(k-1)} = (1/2n)\sum_{i=1}^{m} x^*_{i,k|(k-1)}$

5) State error covariance prediction at time k: $P_{k|(k-1)} = (1/2n)\sum_{i=1}^{m} x^*_{i,k|(k-1)} x^{*T}_{i,k|(k-1)} - \hat{x}^*_{i,k|(k-1)}\hat{x}^*_{i,k|(k-1)} + Q_{k-1}$

// Measurement predictions: calculate measurement predictions, measurement error covariances and cross-covariances //

6) Cholesky decomposition of the updated covariance: $P_{k|(k-1)} = S_{k|(k-1)} S^T_{k|(k-1)}$

7) Calculate volume points: $X_{i,k|(k-1)} = S_{k|(k-1)}\xi_i + \hat{x}_{i,k|(k-1)}$

8) Spread volume points: $Z_{i,k|(k-1)} = h(X_{i,k|(k-1)})$

9) State prediction at time k: $\hat{z}_{k|(k-1)} = (1/2n)\sum_{i=1}^{m} Z_{i,k|(k-1)}$

10) Autocorrelation covariance matrix: $P_{zz,k|(k-1)} = (1/2n)\sum_{i=1}^{m} Z_{i,k|(k-1)} Z^T_{i,k|(k-1)} - \hat{z}_{i,k|(k-1)}\hat{z}^T_{i,k|(k-1)} + R_k$

11) Cross-correlation covariance matrix: $P_{xz,k|(k-1)} = (1/2n)\sum_{i=1}^{m} X_{i,k|(k-1)} Z^T_{i,k|(k-1)} - \hat{x}_{i,k|(k-1)}\hat{z}^T_{i,k|(k-1)} + R_k$

// State Update: calculate Kalman gain, state quantity estimates, error covariance estimates //

12) Filter gain at time k: $W_k = P_{xz,k|(k-1)} P^{-1}_{xz,k|(k-1)}$

13) State estimation at time k: $\hat{x}_{i,k|k} = \hat{x}_{i,k|(k-1)} + W_k$

14) State error covariance estimate at time k: $P_{k|k} = P_{k|(k-1)} - W_k P_{zz,k|(k-1)} W^T_k$

end

Algorithm 1: Iterative Operation Steps of Robust CKF Algorithm.

prediction covariance matrix $P_{k|(k-1)}$ are calculated at each step, which not only greatly increases the amount of calculation, but also easily leads to numerical instability. The aerospace engineering field requires high reliability. In order to overcome the above shortcomings of CKF, the square root filtering idea in the classical KF algorithm is used for reference, and the Cholesky decomposition is introduced on the basis of CKF, and the square root of the covariance matrix is directly propagated and updated in the form of the Cholesky decomposition factor [6–8]. Iterative operation steps of robust CKF algorithm is shown in Algorithm 1.The advantages of introducing Cholesky decomposition are: (1) iteratively update the covariance matrix in the form of the square root of the covariance matrix in the filtering process, which reduces the computational load to a certain extent, and (2) ensure the nonnegative and positive definiteness of the covariance matrix and avoid filtering. It can reduce the divergence of the filter after long-term operation and improve the numerical stability of the filter.

4. Simulation Results and Discussion

4.1. Simulation Flow. There is no a priori model for the attitude change of the spacecraft during the orbital flight. Combined with the overall planning of Chinese manned lunar landing missions, two sets of flight orbit data is simulated, corresponding to the spacecraft's earth-moon transfer orbit. The stable flight period (maximum angular velocity of 4°/s) and the spacecraft's large dynamic attitude adjustment period (maximum angular velocity of 8°/s) are used to verify the tracking performance of the proposed algorithm for the beam angle of the uplink incident communication signal. In order to show the advantages of the proposed robust CKF algorithm compared with similar algorithms in background engineering tasks, the basic CKF algorithm is used as the reference object in the simulation analysis.

The operation flow of the numerical simulation example is shown in Figure 5, including the four-phase modulation and difference beam amplitude generation in Figure 2, the angle observation calculation based on Equations (8) and (9), the angle vector synthesis, and the angle tracking filter output.

4.2. Simulation of Stable Attitude Condition. A nonlinear motion equation is modeled based on beam angle measurement (Equations (8) and (9)):

$$\text{Azimuth state equation}: x_\theta(k+1) = F \cdot x_\theta(k) + \left(\frac{H}{x_\theta(k) + R_k}\right), \quad (11)$$

$$\text{Azimuthobservation equation}: z_\theta(k+1) = a\tan\left(0.1 \cdot x_\theta(1, k+1)\right) + Q_k, \quad (12)$$

$$\text{Pitch state equation}: x_\varphi(k+1) = F \cdot x_\varphi(k) + H/\left(x_\theta(k) x_\varphi(k)\right) + x_\theta(k)\tan\left(x_\theta(k)\right)\tan\left(x_\varphi(k)\right) + R_k, \quad (13)$$

$$\text{Pitch observation equation}: z_\varphi(k+1) = a\tan\left(0.1 \cdot x_\varphi(1, k+1)\right) + Q_k. \quad (14)$$

Related parameter initialization mainly includes the

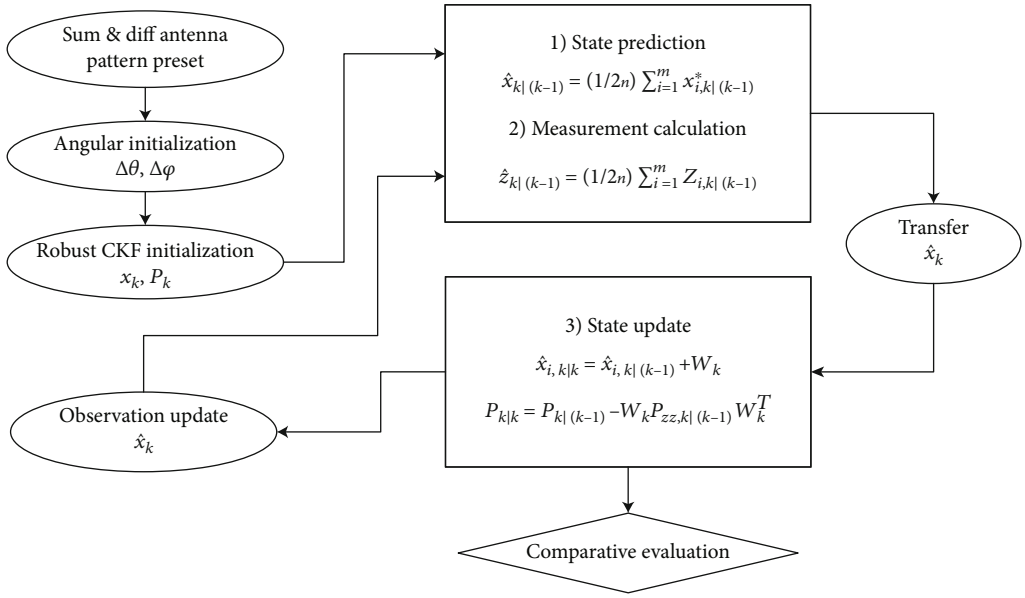

Figure 5: Simulation flow diagram.

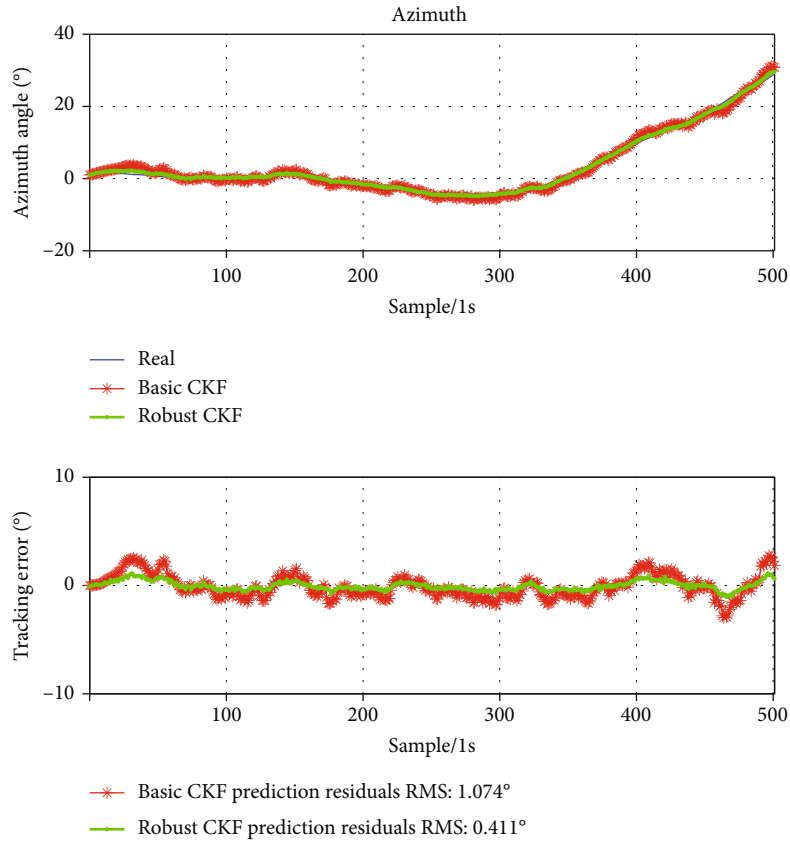

Figure 6: Azimuth tracking results.

following: (1) azimuth φ initial state, $x_\varphi(1) = [1 : 0.1]$; pitch angle θ initial state $x_\theta(1) = [0.1 : 1]$; (2) initial estimate variance $P = [0.0099, 0\,; 0, 0.0001]$; (3) multiplier factor, $F = [1, 1\,; 0, 1]$; (4) phased array antenna constants, $H = \lambda/2\pi$D, $\lambda = 12.7$mm, and $D = \lambda/2$; (5) Gaussian system noise, $Q_k \sim N(0, 0.001)$ and $R_k \sim N(0, 0.16)$; and (6) running points, $N = 500$ and sampling interval 1 second.

The simulation results are shown in Figures 6 and 7. The azimuth and pitch angular velocity are up to 1°/s, and the overall attitude is stable. Both the basic CKF and the

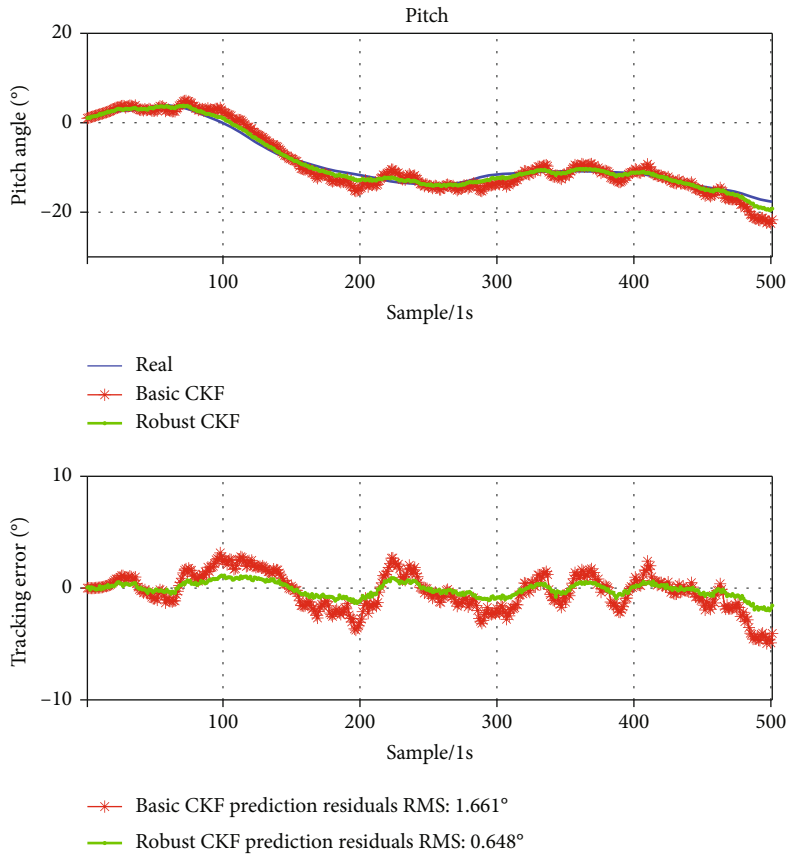

Figure 7: Pitch tracking results.

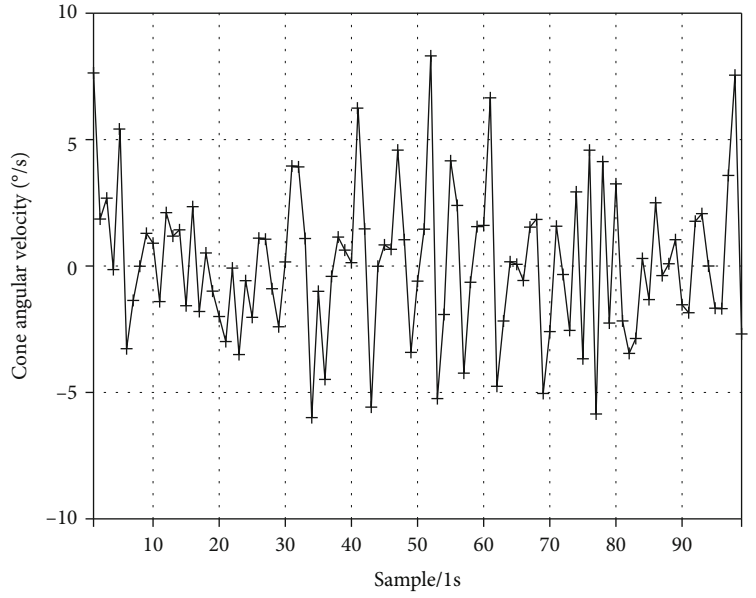

Figure 8: Large dynamic cone angular velocity (combination of azimuth and pitch angle).

improved robust CKF algorithm can achieve continuous tracking. Among them, the tracking filtering performance of the robust CKF algorithm is slightly better, and the residual is relatively small within 1°, which meets the needs of tight beam tracking. The tracking residual of the basic CKF algorithm suddenly increases after running for about 450 s, and the maximum reaches 3.8° with a divergent trend. The robust CKF algorithm has relatively small fluctuations in the same period, the maximum is about 1°, and the stability is relatively good. In terms of time overhead, the basic CKF operation takes 0.042 s per point (per second), while the robust CKF algorithm takes

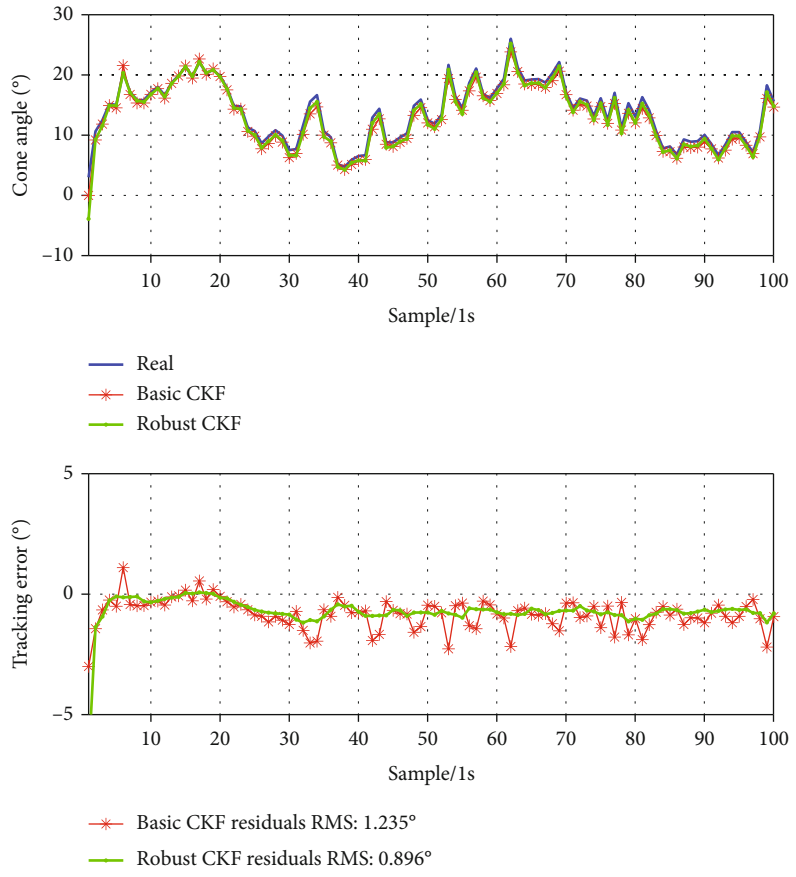

Figure 9: Cone angle tracking results.

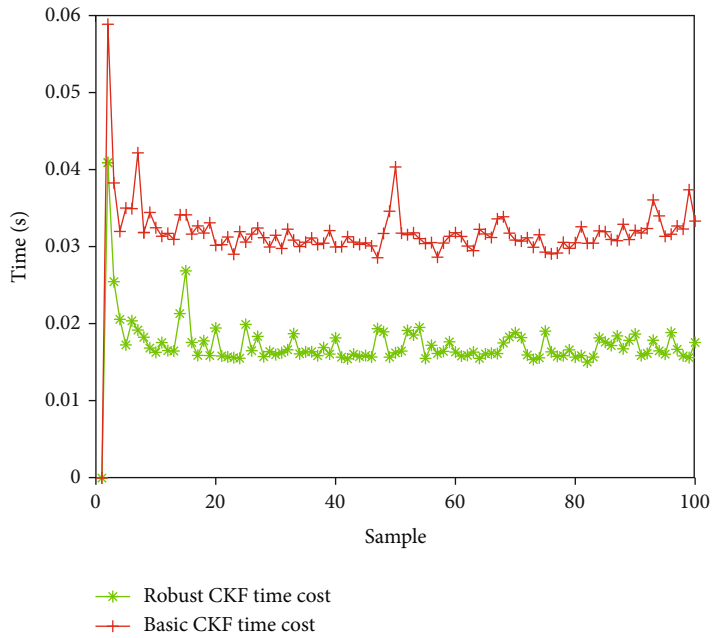

Figure 10: Time-consuming comparison.

about 0.03 s. In terms of computational efficiency, the robust CKF algorithm is superior, which is in line with the theoretical analysis.

4.3. Simulation of Large Attitude Dynamic. Considering that the azimuth and pitch angles are combined into vectors in practical engineering, in this example, the state and

observation equations are established for the combined cone angles [8].

$$\text{State equation}: x_\theta(k+1) = 1 + F \cdot x_\theta(k) + \left(\frac{\sin(0.04\pi k)}{x_\theta(k) + R_k}\right), \tag{15}$$

$$\text{Observation equation}: z_\theta(k+1) = x_\theta^2(k+1)/5 + Q_k, \text{ if } (t < 30)\ z_\theta(k+1) = x(k+1)/2 - 2 + Q_k, \text{ if } (t \geq 30). \tag{16}$$

Related parameter initialization mainly includes the following: (1) initial state of attitude angle, $x_\varphi(1) = 1$; (2) initial estimate variance, $P = 3/4$; (3) multiplier factor $F = 0.5$; (4) phased array antenna constants,$H = \lambda/2\pi$D, $\lambda = 12.7$mm, and $D = \lambda/2$; (5) Gaussian system noise, $Q_k \sim N(0, 1.5)$, and $R_k \sim N(0, 0.1)$; and (6) running points, $N = 100$ and sampling interval 1 second;.

The simulation results are shown in Figures 8–10. During the whole process, the angle changes drastically, and the angular velocity reaches a maximum of 8°/s. Under this condition, both the basic CKF and the improved robust CKF algorithm can achieve continuous tracking. In most of the time periods, the robust CKF algorithm has slightly better tracking and filtering performance, the overall error margin is relatively small, and the RMSE is close to 1°, which meets the requirements of tight beam angle tracking. At the beginning of the simulation, the robust CKF algorithm converges slightly slower, resulting in a maximum angular error of 5°, which is slightly worse than the basic CKF. Figure 10 shows the time overhead of each calculation point of the two algorithms, and the robust CKF algorithm is dominant in terms of operational efficiency.

5. Conclusions

Based on the needs of China's future deep space exploration project, the technical scheme for stable communication to the ground under the condition of spacecraft attitude changes is discussed, and the phased array mono-pulse tracking communication system is proposed as the preferred scheme. The overall scheme and workflow of the phase-type mono-pulse angle measurement technology are systematically introduced, and a simplified mathematical model of angle measurement is proposed, which is convenient for tracking and recursive operation while meeting the accuracy requirements. Aiming at the accurate and stable pointing of the beam in the situation of attitude change, the nonlinear Gaussian filtering algorithm is comparatively studied, and a robustness improvement scheme based on the CKF algorithm framework is proposed. The two-dimensional angle tracking filtering algorithm based on the robust CKF is described in detail. Simulation examples show that the proposed algorithm is better than the basic CKF algorithm in terms of accuracy, efficiency, and robustness, and its comprehensive performance can meet the needs of future engineering tasks. The research results can provide reference for engineering implementation in related fields in my country in the future.

Data Availability

A data availability statement is already included in my manuscript.

Conflicts of Interest

There is no conflict of interest regarding the publication of this paper.

Acknowledgments

This study has been supported by the Aerospace Innovation Fund (21GFH-HT01-36).

References

[1] Z. Lin, *Research and Implementation of Monopulse Angle Measurement and Difference Beamforming Algorithm*, Nanjing University of Science and Technology, 2018.

[2] D. Jia-lin, X. Jian, and Z. Tao, "Adaptive CKF strong tracking filter and application," *Journal of Electric Machines and Control*, vol. 19, no. 11, pp. 111–120, 2015.

[3] W. Xi-qing and S. Shen-min, "Model-free cubature Kalman filter and its application," *Control and Decision*, vol. 28, no. 5, pp. 769–773, 2013.

[4] S. Feng and T. Lijun, "Estimation precision comparision of cubature Kalman filter and unscented Kalman filter," *Control and Decision*, vol. 28, no. 2, pp. 303–308, 2013.

[5] I. Arasaratnam and S. Haykin, "Cubature Kalman filters," *IEEE Transaction on Automaitc Control*, vol. 54, no. 6, pp. 1254–1269, 2009.

[6] X. C. Zhang and C. J. Guo, "Cubature Kalman filters: derivation and extension," *Chinese Physics B*, vol. 22, no. 12, article 128401, 2013.

[7] X. C. Zhang and Y. L. Teng, "A new derivation of the cubature Kalman filters," *Asian Journal of Control*, vol. 16, no. 5, pp. 1501–1510, 2014.

[8] X. C. Zhang, "Cubature information filters using high-degree and embedded cubature rules," *Circuits, Systems, and Signal Processing*, vol. 33, no. 6, pp. 1799–1818, 2014.